Structures 53 (2023) 1435–1449

Contents lists available at ScienceDirect

Structures

journal homepage: www.elsevier.com/locate/structures

A novel fully removable walkway system with non-invasive anchors for structural health inspection and maintenance of historic steel structures

Manuel Cabaleiro [a,b,*], Borja Conde [b], Cristina González-Gaya [a], Brais Barros [b]

[a] Department of Construction and Manufacturing Engineering, Universidad Nacional de Educación a Distancia (UNED), Spain
[b] Department of Materials Engineering, Applied Mechanics and Construction, School of Industrial Engineering, University of Vigo, Spain

ARTICLE INFO

Keywords:
Historic steel constructions
Maintenance & inspection
Steel trusses
Historic steel bridges
Non-invasive connections
Laser scanning

ABSTRACT

Historic steel structures are generally heritage constructions that must be preserved, where invasive operations such as welding or drilling cannot be performed. Any auxiliary structures installed on these constructions must be easily removable. In addition, historic steel structures such as riveted bridges are difficult to access, making it very difficult to take measurements using contact techniques or to perform structural health inspections. One of the most common needs is the installation of walkways for inspection and especially for maintenance and repair purposes. In this sense, clamp-based connections are a technique for fabricating dismountable systems that allow anchoring to existing structures without performing invasive operations such as welding or drilling. This study proposes, develops, simulates, and tests a novel non-invasive detachable anchorage system for the assembly of temporary walkways for inspecting and maintaining historic steel structures without additional scaffolding. In addition, a methodology is proposed for the easy and correct installation of the proposed system by combining it with LiDAR techniques. The developed system has been assembled and tested in laboratory tests and two real case studies.

1. Introduction

Nowadays, there are a large number of steel structures and buildings that are more than a century old. These buildings include, for example, railway stations or bridges. Many of these historic buildings are still in service, either maintaining their original use or being converted for a new purpose (Fig. 1). One of the major problems of steel structures is corrosion damage over time [1–6]. Therefore, these buildings require maintenance actions and periodic structural health inspections [7,8]. Due to the location and height of these types of buildings, it is usually necessary to suspend regular service for several days for temporary inspection and maintenance. In addition, it is often necessary to erect additional scaffolding or use climbers, especially on the outside of the building where there are usually no fixed walkways.

Thus, one of the current needs for temporary inspection, maintenance, and repair work in steel construction (especially for the external parts of a bridge) is to have easily removable walkways without interrupting the construction service and without having to use climbers since it is becoming increasingly difficult to find qualified inspection personnel with skills for working at height at an affordable cost, in addition to the human risk involved. As already mentioned, these constructions are difficult to access, so the system developed must allow the platform to be assembled and disassembled on itself, and a single person must easily manipulate each element to be used. These walkways could also be used for temporary pedestrian access if permitted by applicable historic preservation regulations.

The historical steel structures have several geometric characteristics that must be taken into account for any secondary structure to be anchored to them; among these characteristics, it is worth mentioning that: (a) these structures were made by riveted connections of plates and angle sections, so their dimensions are not standardized; (b) the thickness of the flanges of the main chords varies along the length of the member; (c) each structure has different cross-sectional dimensions of the beams, especially the main chords of the trusses; (d) on the outer faces of the main steel members, the heads of the rivets are usually present, so the surface is not entirely smooth.

There are currently several joining systems for steel buildings, some permanent, such as welding, and some removable, such as bolting [9,10]. However, all require invasive operations. Clamp-based connection systems are ideal for fabricating removable and reconfigurable steel structures that can be anchored to existing structures without prior operations [11–14].

* Corresponding author at: Department of Construction and Manufacturing Engineering, Universidad Nacional de Educación a Distancia (UNED), Spain.
E-mail addresses: mcabaleiro@uvigo.es, mcabaleir15@alumno.uned.es (M. Cabaleiro).

https://doi.org/10.1016/j.istruc.2023.05.019
Received 13 February 2023; Received in revised form 4 April 2023; Accepted 6 May 2023
Available online 13 May 2023

Nevertheless, for installing any new structure on the existing one, even with removable systems such as clamps, it is necessary to know in advance the geometric dimensions, including the position of the rivets, so that they do not interfere with the new profiles. As mentioned above, the main problem with this type of construction is the difficulty of access, especially when it is in operation. A promising solution to obtain measurements of existing buildings is LiDAR (Laser Imaging Detection and Ranging) techniques, especially laser scanning. Laser scanning is a state-of-the-art technology that allows obtaining geometric measurements of any object from a distance without the need to come into contact with it. Among the most common applications of laser scanning in construction, we can include documentation of historical buildings [15–18], 3D modeling of buildings for structural analysis [19–22], and structural health analysis [23–28].

This work aims to develop systems and methodologies that, by combining non-invasive dismountable connection systems with LiDAR techniques, allow the installation of easily assembled and disassembled walkways for structural health inspection, maintenance, repair, or accessibility in historic steel structures without the need for additional scaffolding. FEM simulations and experimental (laboratory) tests will be performed on the proposed system to verify its mechanical behavior. Finally, it will be applied to two case studies by extracting the geometric dimensions using LIDAR techniques and assembling a module of the developed walkway.

The work presented below is divided into three parts. In the first part, the proposed walkway and the anchorage system are described (section 2), then the laboratory tests performed on the anchorage system are presented (section 3), as well as the FEM simulations and their results (section 4). In the second part, the proposed methodology for installing the walkway on existing structures from LiDAR data is described (section 5), and then the case studies where this methodology is applied are shown (section 6). Finally, conclusions are drawn in the last part (section 7).

2. Proposed anchoring and walkway system

When designing this new system of inspection walkways, it was considered that they should generally be located on the outside of the structure since, in many cases, either maintenance walkways are already installed inside or access to this area is usually easier. On the other hand, the walkways should be located in the lower part of the structure since, from this area, it is easier to access the upper points of the structure employing, e.g., a ladder. Therefore, the anchorage of the walkways should be placed mainly in the lower steel members (e.g., lower chords in a truss bridge).

2.1. System description

The system developed consists of L-shaped profiles, cantilevered and anchored with two clamps to the flanges of the lower chord of the trusses (Fig. 2). These clamps are adjusted in height by extensions according to the thickness of the profile flange to which they are anchored since it is common in historical structures that the number of steel plates used in the chords varies along their length. On the other hand, to ensure that the walkway is a level surface (since the height position of the upper surface of the L-type profile anchored to the bridge varies according to the thickness of the flanges of the lower truss chords), the L-type profile is provided with a regulating and reinforcing plate fixed with several bolts and nuts through slotted holes. The slotted holes allow the height to be adjusted, leveling the platform surface and securing its position by tightening the appropriate bolts and nuts connecting the L-type profile.

It should be noted that the flange of the L-profile must have a maximum width so that it can always be placed between two rows of rivet heads, and it must also have a limited depth so that it does not exceed the maximum weight that the operator can handle. The cross-sectional dimensions of the L-profile are therefore bounded, and consequently, so is its bending capacity. The adjustment plate is designed to allow (in addition to the height adjustment) the reinforcement of the L-beam to withstand the bending stresses due to maintenance loads. Thanks to the walkway's design, the assembly process can be carried out progressively by a single person without the need for scaffolding or additional lifting equipment.

It is also common for these structures to have gusset plates inside the chords, which would prevent the placement of clamps (Fig. 3a). In these cases, a countersunk plate with a countersunk bolt and nut would be placed on the L-beam to act as a stop against the flange of the truss chord. On the other hand, the clamp (2) used would be provided with threaded holes in which two horizontal bolts would be placed, which

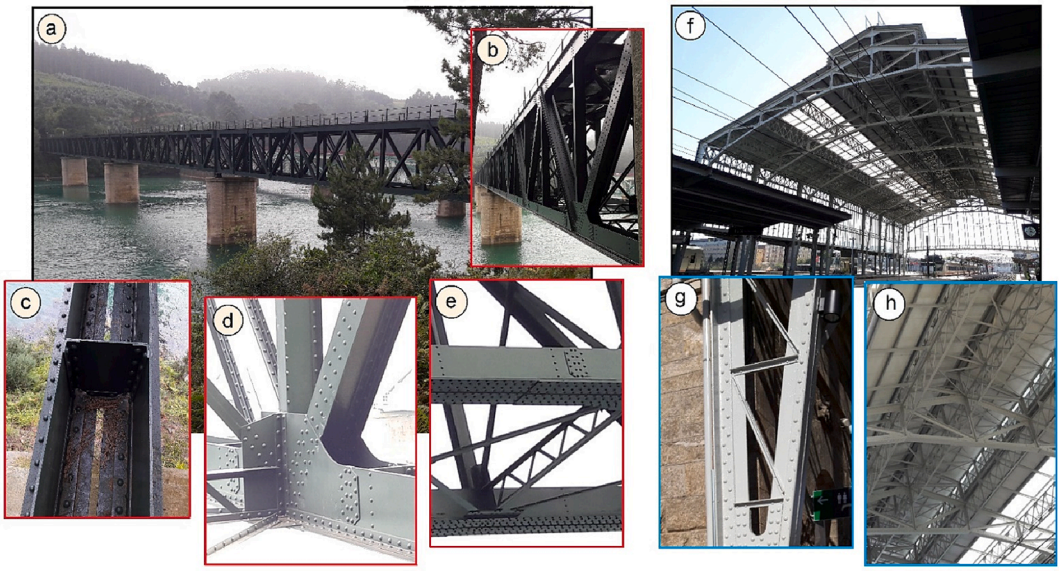

Fig. 1. a) Example of a historic steel railway bridge in service b) Detail of the exterior of the structure, which is very difficult to access c) Lower chord where new structures can be anchored using a clamp-based connection system d) Detail of the interior of the bridge showing the connection between the gusset plate and the lower chord e) Detail of the rivet heads on the underside of the bridge chords f) Example of a historic steel building currently in use as a railway station g) Detail of the riveting of the profiles of a column h) Detail of the roof truss.

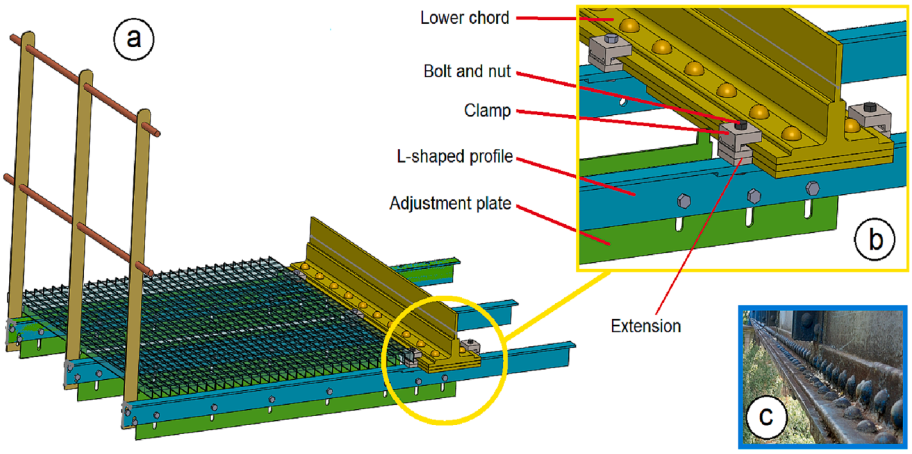

Fig. 2. 3D view of the developed walkway system a) Platform module mounted on a truss chord b) Detail of the L-shaped profile, adjustment plate, and clamps c) Detail of the flange of a truss chord.

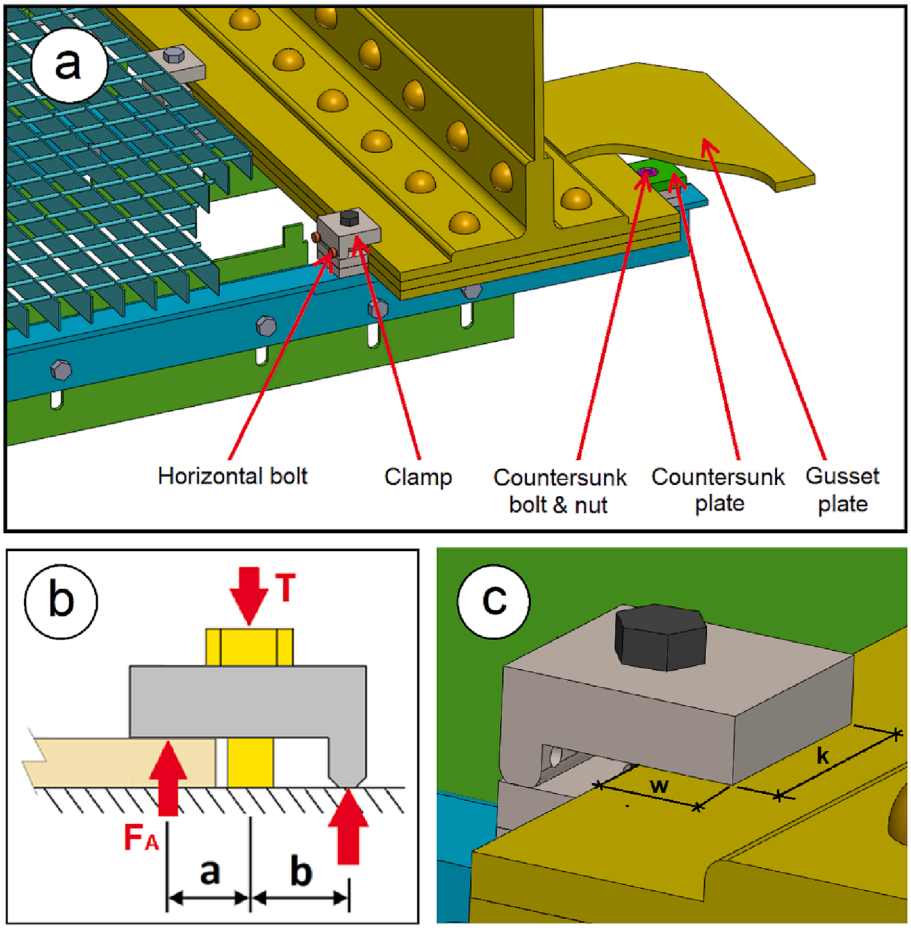

Fig. 3. a) Detail of the assembly when there is interference with a gusset plate. b) Working mode of the clamp by the leverage mechanism c) Detail of the surface support of the clamp on the bridge profile flange.

would ensure positioning by means of the pressure exerted during tightening against the flange of the chord, butting against the countersunk plate 10.

The preload (T) of the clamp bolt shall be applied according to Eurocode 3 [29]; see equation (1):

$$T = \frac{0,7 f_{ub} A_s}{1,1} \quad (1)$$

where f_{ub} is the ultimate tensile strength of the steel bolt, and A_s is the net cross-section area of the bolt.

The clamps work by the leverage mechanism (see Fig. 3b) so that according to the preload applied to the bolt (T), a force (F_A) will appear on the surface of the clamp, which rests on the flange of the profile, as shown in the following expression:

$$F_A = \frac{T \bullet b}{a + b} \quad (2)$$

Thus, the pressure exerted on the profile flange surface will be equal to this force F_A distributed on the support surface, which is equal to the clamp width (k) and depth (w) (see Fig. 3c). The clamp must be dimensioned so that this pressure does not damage the coating system and lead to corrosion. In addition, a reinforced plastic sheet could be applied between the surfaces of the clamp and the web to ensure better support and to avoid possible damage.

2.2. Assembly process

The steps to assemble the walkway are as follows (Fig. 4): 1) Place the first two L-beams with their anchoring clamps on the bottom chord of the truss. The distance between the beams will be approximately 400 mm (adjustable according to the distance between the rivet heads). The adjustment plates are then positioned according to the lowest level allowed. This short distance between the L-beams and the low weight of each walkway component allows them to be assembled by a single person 2) Placement of a first 500 mm wide grating module anchored to the L-beams 3) Placement of a third beam and adjustment plate at a distance of approximately 400 mm from the last beam 4) Replacement of the 500 mm wide grating module with a 1000 mm wide one 5) Placement of two new L-beams and adjustment plates. The distance between the last beam and the next one will be about 200 mm, and the distance between the two new beams will be about 400 mm (adjustable according to the distance between the rivet heads) 6) Place a 500 mm wide grid module 7) Place a new beam and its adjustment plate about 400 mm from the previous one 8) Replace the 500 mm wide grid module with a 1000 mm wide one 9) Repeat steps 5, 6, 7 and 8.

2.3. Loads to be supported

As this design is a special system for a specific application, the maximum loads to be withstood are not dictated by specific codes but must be adapted to those generally used for inspection and maintenance. In this case, the point loads required by Eurocode 1 [30] for roof maintenance are used as a reference. This is a concentrated load of 1.0 kN at the most unfavorable point, i.e., the cantilever end of the L beam. It is also calculated with a distributed load on the beam of 2.4 kN. This load would correspond to three persons or two persons plus a load of approximately 800 N. The safety factor is specified in Eurocode 0 [31] for variable loads, i.e., 1.5.

3. Laboratory tests

Several laboratory tests were carried out to analyze the mechanical behavior of the proposed system, both in terms of strength and deformation (Fig. 5). The experimental results obtained allowed the validation of the developed FEM computational model.

3.1. Laboratory-tested support beams

The prototype beams tested consisted of an L-section with cross-sectional dimensions of 50x80 mm, a thickness of 6.0 mm, and a length of 1500 mm (Fig. 5). The main beam was a corroded HEB 300 profile with a flange width of 300 mm (minimum width -usually- of the plates used as flanges in the lower chords of historic riveted steel truss bridges) with a length of 1000 mm, and a thickness of 14 mm. The L-beam was connected to the bottom flange of the HEB using clamps, bolts, and nuts. In addition, a 4.0 mm thick adjustment plate with 50 mm shaved holes was mounted to the side face of the L-beam. S235 steel was used for the profiles, plates, and clamps. M12 metric and 8.8-grade bolts

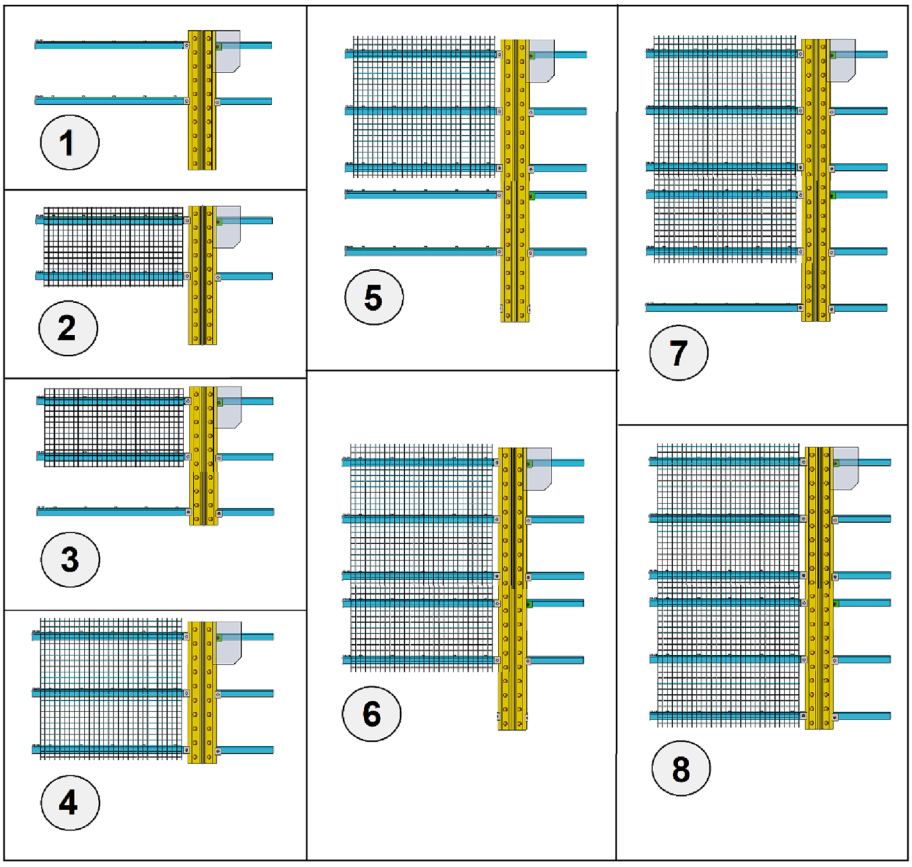

Fig. 4. Assembly process of the walkway system.

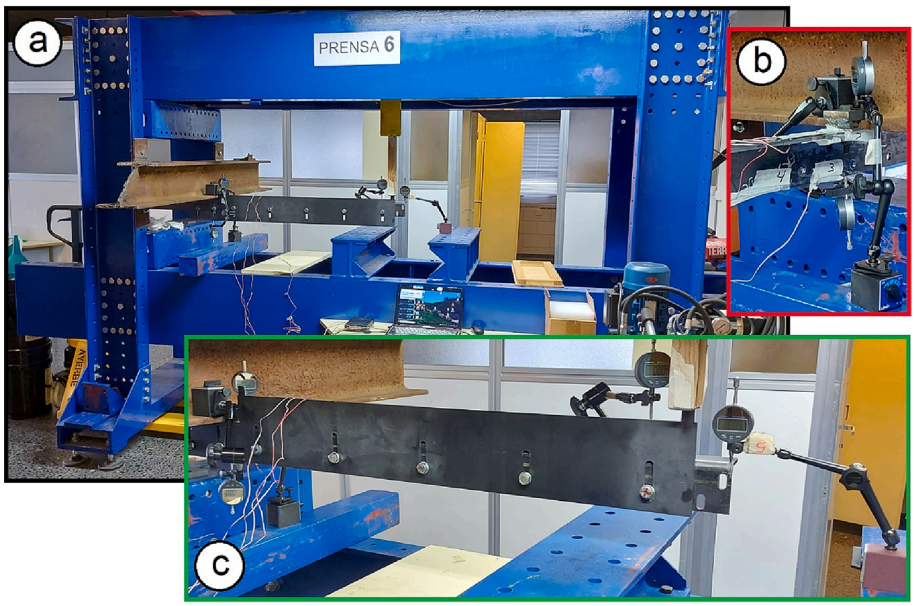

Fig. 5. Laboratory tests a) Assembly of the anchorage system with the adjustment plate at the bottom b) View of the L-beam connection with the HEB profile without the adjustment plate c) Detail of the positioning of the digital indicators with the adjustment plate at the top.

were used. These were tightened using a torque wrench with a preload of 36 kN.

The displacements at the end of the L-beam (C1) and in the anchorage area of the clamp with the HEB 300 profile (C3) were measured using digital comparators (+/- 0.01 mm). The relative displacements between the L-beam and the adjustment plate (C2) and between the L-beam and the HEB 300 profile (C4) were also measured (see Fig. 6). Prior to the experimental tests, several numerical simulations were carried out with the FE model to determine the areas where the maximum stresses would develop. Based on these results, strain gauges were placed at the most critical points of the L-beam. Strain was therefore measured at the top of the L-beam in the areas close to the clamp bolt hole (B1 and B2) and at the bottom of the L-beam in the area close to the two holes of the bolts connecting it to the adjustment plate (B3 and B4). The parameters of these strain gauges were 6.0 mm long by 4.0 mm wide, a gauge factor of 2.16, and a resistance of 120,000 Ω. The equipment used to collect the strain gauge data was a D4 Micro-measurement [32] with all the gauges arranged in a quarter bridge configuration.

3.2. Experimental results

The results of the laboratory tests were:

(a) L-beam with the adjustment plate positioned at the maximum height allowed by the slotted holes and point load applied at the end. The results obtained are shown in Figs. 7 and 8. The maximum stress is reached in the area of gauge B1 but without exceeding the yield point. The deflection achieved with a load of 1.0 kN was 11.4 mm.

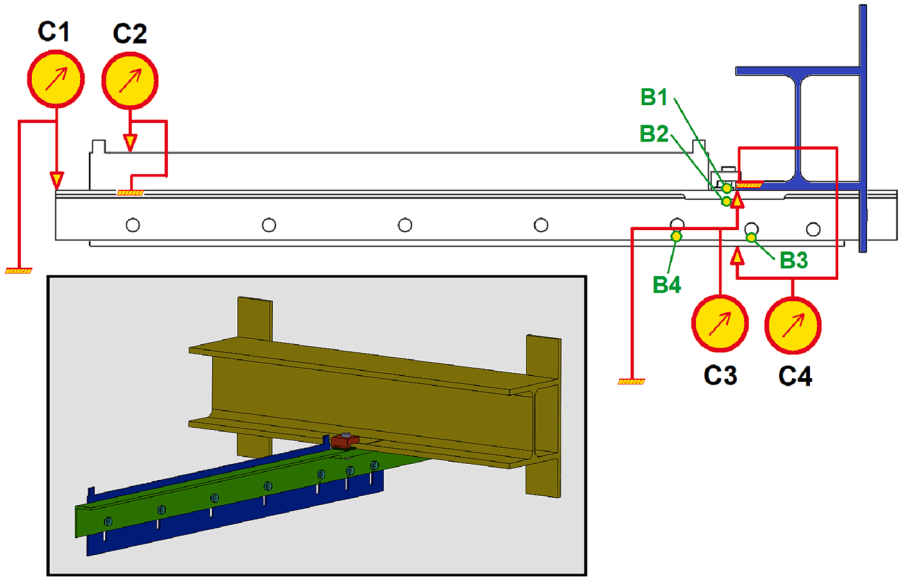

Fig. 6. Scheme of the measuring points using digital comparators and strain gauges, including a 3D view of the anchorage system being mounted on an HEB 300 profile.

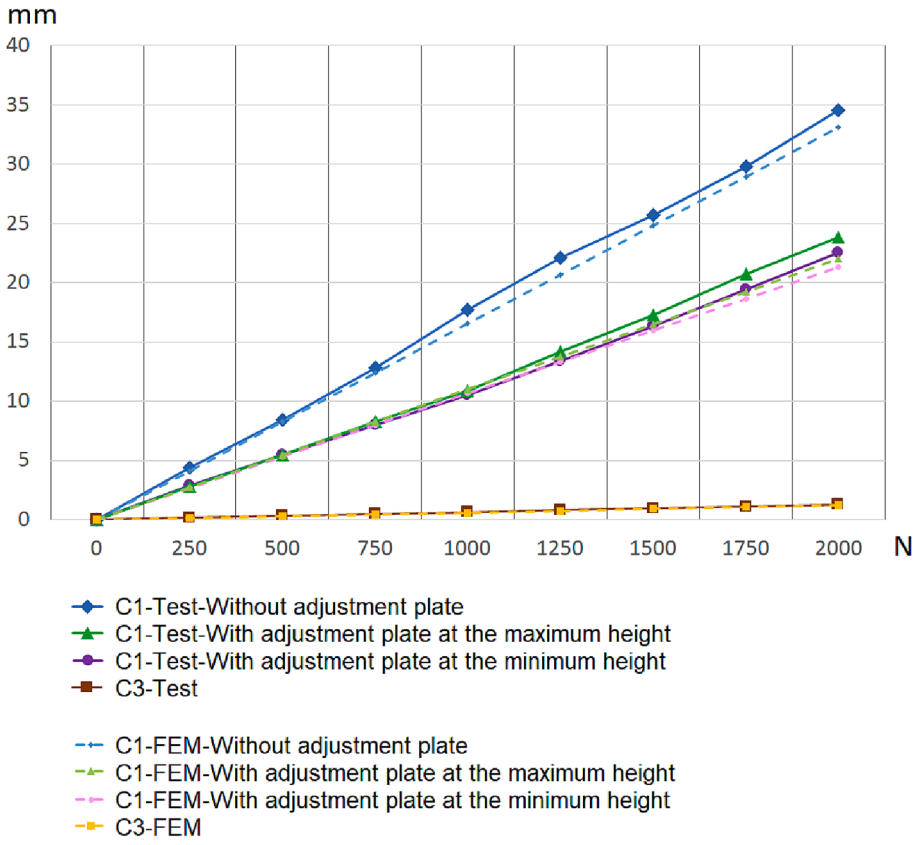

Fig. 7. Graph of the L-beam displacements at points C1 and C3 according to the experimental tests.

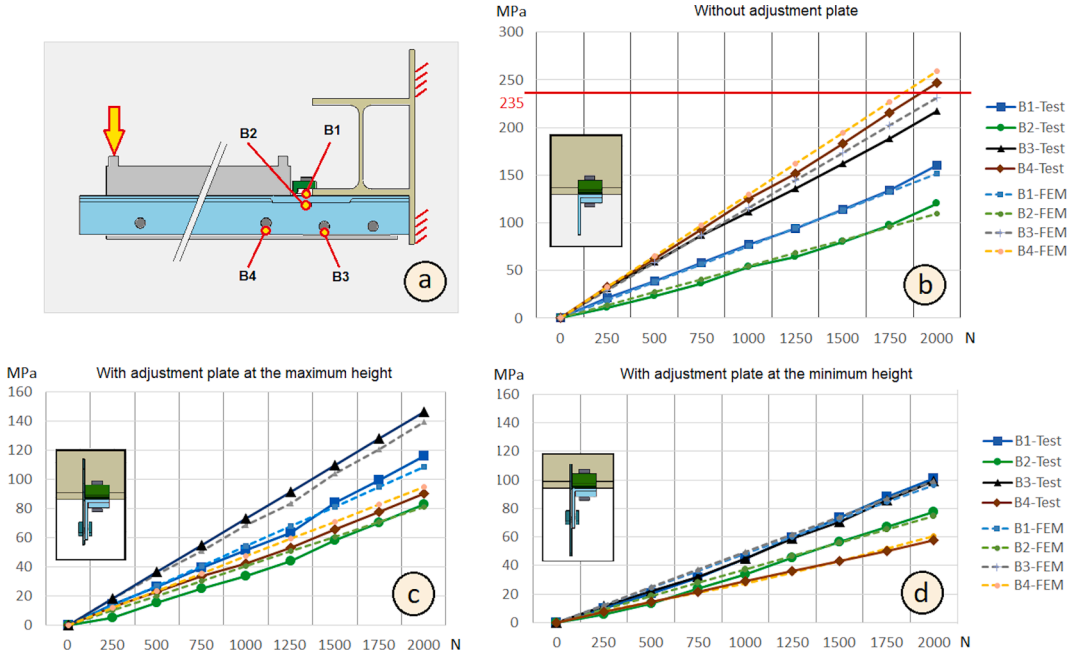

Fig. 8. a) Outline of the measuring points according to the position of the strain gauges. b) Stresses for the L-beam without adjustment plate c) Stresses for the L-beam with adjustment plate at the maximum height d) Stresses for the L-beam with adjustment plate at the minimum height.

(b) L-beam with the adjustment plate placed at the minimum height allowed by the slotted holes and a point load applied at the end. The results obtained are shown in Figs. 7 and 8. The maximum stress is reached in the area of gauge B1 but without exceeding the yield point. The deflection obtained at a load of 1.0 kN was 12.3 mm.

(c) L-beam without adjustment plate and point load applied at the end. The results obtained are shown in Figs. 7 and 8. The deflection obtained with a load of 1.0 kN was 19.3 mm. When a

load of 2.0 kN was applied, the yield strength of the material was exceeded in the area of gauge B4, and a permanent deflection of 2.4e05 was measured.

Furthermore, there was no slippage between the adjustment plate and the L-beam (measurement C2) in all cases. On the other hand, in all cases, the deformation obtained in the HEB 300 after applying the load at point C3 was the same.

3.3. Assembly of the platform in the laboratory

After testing the prototype beams, a 2-meter section of the platform was assembled to verify its functionality in the laboratory (seeFig. 9). Assembly was satisfactory and could be carried out by one single person due to the design and weight of each element that makes up the platform.

4. Numerical model

A 3D Finite Element (FE) model was developed to simulate the mechanical response of the proposed anchorage system under different load actions (Fig. 10). The modeling process was performed using the ANSYS [33] software package.

4.1. FE model

Solid bodies were used for the geometric modeling, considering the same elements used in the experimental tests. For the mesh, second-order hexahedral elements were used for the bolts, while second-order tetrahedral elements were used for the other components due to their more complex shapes and holes. A characteristic finite element size of 30.0 mm was used for the HEB beam, 10.0 mm for the L-beam and adjustment plate, 5.0 mm for the clamps, and 4.0 mm for the bolts. In the strain gauge zones B1-B4, partitions were made in the L-beam of the gauge size to extract the average stresses and compare them with those obtained in the laboratory tests. The total number of elements and nodes was 43,021 and 90,722, respectively.

The material for the clamps, steel members, and plates was structural steel S235 (yield strength: 235 MPa, Young's modulus: 200 GPa, Poisson's ratio: 0.30, and density: 7850). kg/m3). The material considered for the bolts was also steel (grade 8.8) (yield strength: 640 MPa, Young's modulus: 200 GPa, Poisson's ratio: 0.30, and density: 7850 kg/m3). The bolts were preloaded with a load of 36.0 kN. A classical Coulomb friction model was used for the contact surfaces with a friction coefficient of 0.2 (untreated steel surfaces according to standards EN 1090-2:2018 [34] and EN 1993-1-8:2005 [29].

Fig. 9. 2-meter section of the platform system assembled in the laboratory.

4.2. Simulations performed

Each component was calculated for deformation (point load of 1.0 kN and distributed load of 2.40 kN) and resistance (point load of 1.5 kN and distributed load of 3.6 kN). Simulations were also performed for a point load of 2.0 kN, which exceeded the yield strength of the material when no adjustment plate was included in the system assembly (see Section 3.2). The simulations also considered the case where the edge of the HEB profile is considered fixed in order to determine the deformation due to the anchorage system alone. All cases were verified with two different beam flange thicknesses of 14 mm and 44 mm. The simulated combinations are shown in Table 1.

4.3. Results and discussion

The results obtained in terms of displacements are shown in Fig. 11. It should be noted that the deformation obtained in the L-beam when considering the free flange edge with respect to the fixed flange edge, is much higher due to the deformation of the beam flange itself. It should be noted that this deformation always depends on the beams of the structure to which the walkway system is anchored. For the case of the fixed flange edge, a point load of 1.0 kN and considering only the L-beam, the displacement at the end of the L-beam is 10.0 mm, while with the free flange edge, it is 16.0 mm. Fig. 7 shows that the difference in displacement between the experimental results and the FEM simulations has an average deviation of 5.0%, with a maximum of 9.0%, indicating that the numerical model reasonably reproduces the mechanical behavior of the system.

The actual values due to the deformation of the anchorage system formed by the L-beam and the adjustment plate are those obtained with the HEB beam with the flange edge fixed. In this case, it was found that for a point load of 1.0 kN, the deformation with only the L-beam is 10.0 mm, while when the adjustment plate is used at the highest part, it is 4.2 mm, and when it is used at the lowest part, it is 4.4 mm. Therefore, using the adjustment plate reduces the deflection to less than half. These differences are maintained when the HEB flange thickness is 44 mm (see Fig. 11).

In terms of stresses, if only the L-beam is used, the system does not exceed the yield strength at a point load of 1.5 kN. However, with a load of 2.0 kN, the beam exceeds the yield strength of the material in the area of gauge B4 (Fig. 12c and 13). In the case of the beam with the upper adjustment plate, the maximum stresses occur in the region of gauge B3, while in the case of the lower adjustment plate, the maximum stresses occur in the region of gauge B1 (see Figs. 12 and 13). The beam was also simulated without the adjustment plate and slotted holes, but in this case, for a load of 2.0 kN, the yield point is exceeded in the area of gauge B4.

Through these simulations, the correct behavior of the anchorage support on the profile was verified according to the service loads, but since the profile of the lower chord of each truss is usually different on each bridge, a prior calculation must be performed to verify that the profile flange will support the loads transmitted by the platform.

5. Methodology for walkway assembly on historical steel constructions from LIDAR data

The proposed methodology (Fig. 14) is based on the combination of LIDAR techniques, which provide geometric data of historical buildings with tolerances of +/- 2 mm, and the installation process of this type of

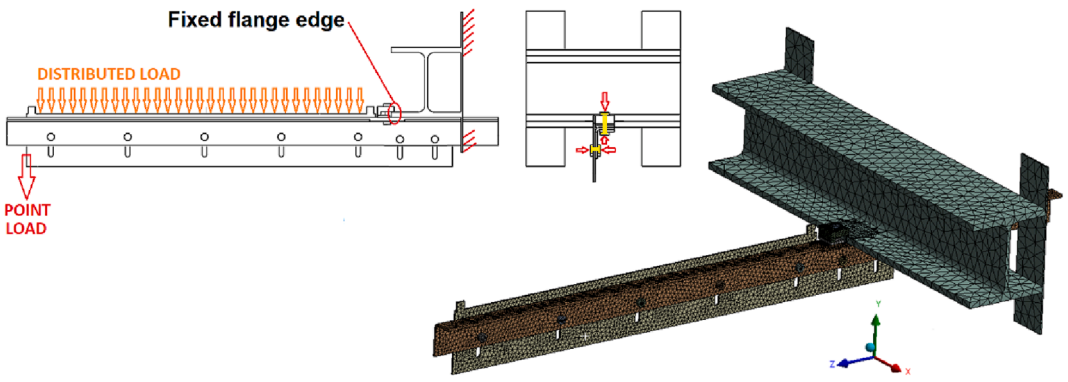

Fig. 10. Scheme of the 3D FE model used for the mechanical analysis of the system behavior.

Table 1
Simulations performed with the FE model.

	Point Load			Distributed Load		
	(H14) Flange thickness 14 mm		(H54)	(H14) Flange thickness 14 mm		(H54)
	Free flange	Fixed flange	Free flange	Fixed flange	Free flange	Fixed flange
With the adjustment plate placed at the maximum height	X	X	X	X	X	X
With the adjustment plate placed at the minimum height	X	X	X	X	X	X
Without the adjustment plate placed	X	X	X	X	X	X
Without the adjustment plate and tears	X			X		

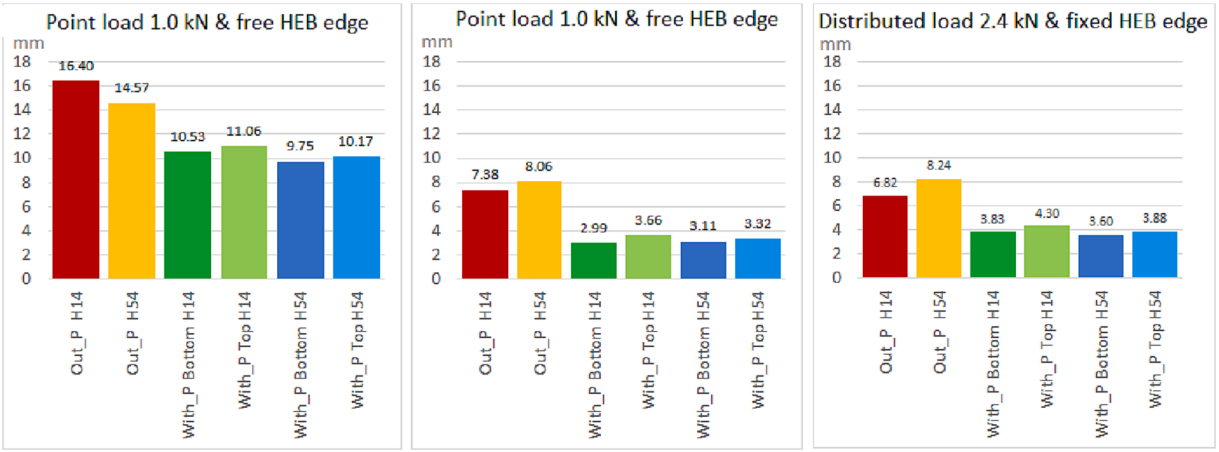

Fig. 11. Graphs of the deflection values at the end of the L-beam (C1) a) Point load at the end of 1.0 kN and free HEB edge b) Point load at the end of 1.0 kN and fixed HEB edge c) Distributed load across the beam of 2.4 kN and fixed HEB edge.

walkways with removable and non-invasive anchors, which allow easy adjustment and adaptation to different thicknesses and positions of the structure. The methodology is carried out through the following steps:

5.1. Scanning of the construction

Fieldwork consists of scanning the construction from different positions, especially those that allow obtaining the geometry of the lower area of the structure.

5.2. LiDAR point cloud data processing and analysis

After scanning with a terrestrial laser scanner, each point cloud is analyzed. The following measurements, among others, are obtained from the point clouds: a) width of the beams of the lower chords of the trusses b) thickness of the flange of the beams where the anchorage system will be positioned c) position and spacing of the rivets d) position and location of the gusset plates that may interfere with the anchorages. To later develop the complete 3D model of the structure, it is necessary to register the different point clouds of each scan into a single global point cloud with a single reference system. This process is called registration, and it involves creating a single file of the entire structure and removing anything from the global point cloud that is not part of the structure, such as noise or unwanted features like vegetation.

5.3. 3D modeling of the construction and previous verifications

From the geometric measurements obtained by laser scanning (and,

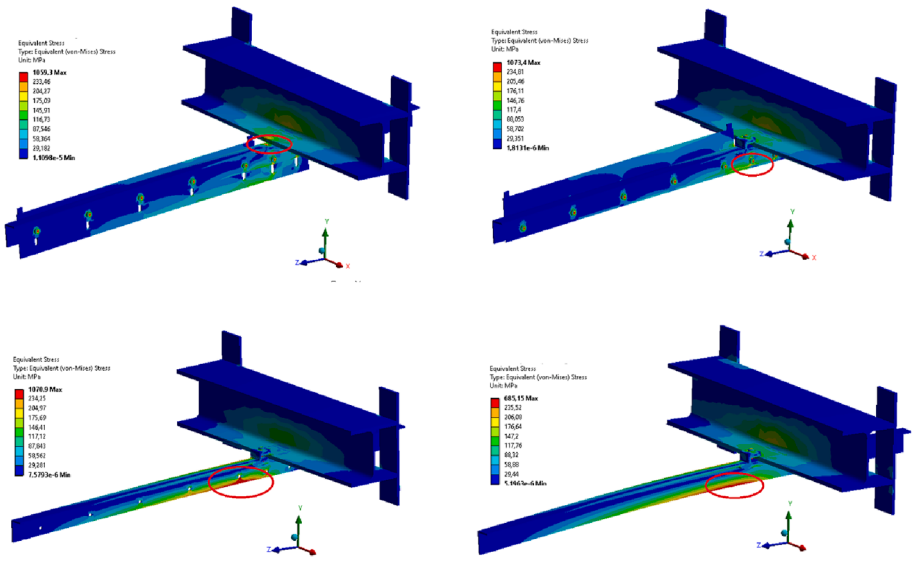

Fig. 12. Stress distribution for a point load of 2.0 kN at the end of the L-beam a) L-beam with adjustment plate on top b) L-beam with adjustment plate on bottom c) Only L-beam with slotted holes d) Only L-beam without slotted holes.

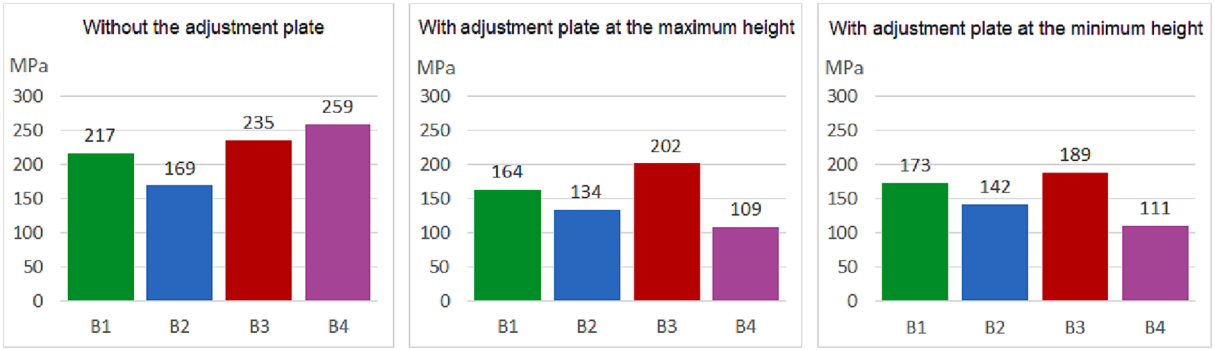

Fig. 13. Plots of stress values for a point load of 2.0 kN at the end of the L-beam a) Stresses for the beam without the adjustment plate b) Stresses for the beam with the adjustment plate at the maximum height c) Stresses for the beam with the adjustment plate at the minimum height.

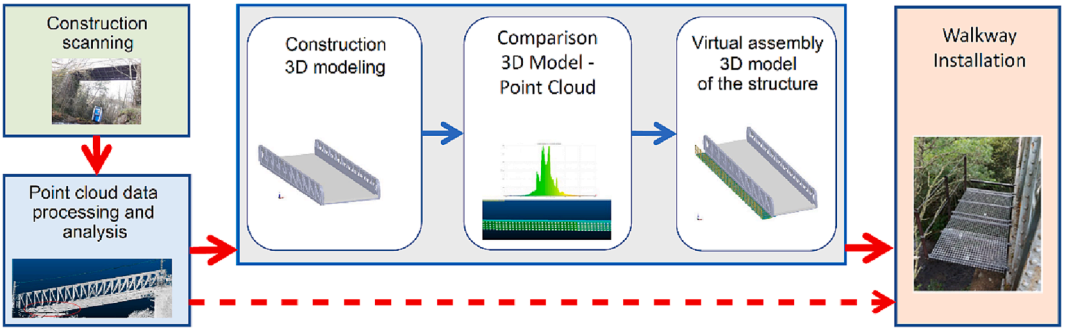

Fig. 14. Outline of the methodology for walkway assembly on historical steel constructions from LiDAR data.

if necessary, supplemented by some manual measurements on site in easily accessible areas), the 3D model of the structure can be developed. At this stage, it is also possible to verify the consistency of the 3D model with the point cloud. To do this, the parts of the 3D model to be verified are exported in a format compatible with the point cloud processing software, then the 3D model is aligned with the point cloud, and finally, the error between the point cloud and the geometric CAD (Computer Aided Design) model is compared using some suitable error measurement tools. Before assembling the walkways on the actual structure, the virtual assembly of the 3D model of the structure and walkway is performed to verify that there are no possible interferences or errors. Due to the adaptability of the system developed, for structures that are not very complex, step 5.3 can be omitted, as the measurements obtained in step 5.2 are sufficient to determine the components necessary to carry out the walkway installation.

5.4. *Installing the walkways for inspection and maintenance purposes*

Finally, the walkway is installed on the historic steel structure, following the steps outlined in Section 2. This allows the necessary

inspection and maintenance work to be carried out without the need for additional scaffolding.

6. Case studies

The developed system was installed in two real case studies using the proposed methodology to verify its correct operation. First, in an easily accessible bridge, such as the steel bridge over the Gadanha River (Lapela) in Portugal, an aging bridge currently used exclusively by pedestrians. Then, the Fillaboa Bridge is considered, which is currently used by the railway but is difficult to access and requires a structural health analysis due to its current corrosion state.

6.1. Bridge over the Gadanha river

The steel bridge over the Gadanha River was part of the railway line between Valença and Monçao in Portugal, inaugurated in 1915 (Fig. 15). The railway was closed in 1989, and since 2004 it has been converted into a greenway and is now used for pedestrian and cycle traffic. The bridge consists of a single span 5.0 m wide, 1.7 m high, and 20.0 m long. The bridge is made of riveted steel, consisting mainly of plates and L-shaped profiles. The width of the profiles of the lower chords of the trusses is 300 mm, with a flange thickness of 24.0 mm in the middle third of the trusses and 12.0 mm at the ends.

6.1.1. Scanning of the construction

The Faro Focus 3D X 330 [35] terrestrial laser scanner was used for digitizing the structure and obtaining its geometric measurements. This laser scanner model measures distances from 0.6 m to 120 m with a nominal accuracy of ± 2.0 mm. A total of eight different scans were performed (see positions in Fig. 16), with an average number of points per scan of 22,571,458, although the actual number of points belonging to the bridge was only 3,299,486 on average. CloudCompare software was used to post-process the point cloud.

6.1.2. LiDAR point cloud data

From the point cloud (Fig. 17), the main measurements of the structure and its components were derived to verify the adequacy of the walkway to the bridge. To create the bridge 3D model, the point clouds were merged into a single global point cloud. Six scans were used for this purpose, resulting in a total of 29,610,362 points.

6.1.3. 3D modeling of the construction

Based on the point cloud of the bridge, 3D CAD modeling was performed using Solidworks 2021 software (Fig. 18). Similarly, the developed detachable walkway system was assembled into the 3D model of the bridge to verify its adaptability.

6.1.4. Installation of the walkway

The entire platform system was assembled and anchored by a single person, and the steps followed are those indicated in the methodology in Section 2, although some simplifications have been made in this case as it is a case study to test the assembly of the walkway.

First, the first three L beams were anchored to the bridge as access to the third beam was easy without having to attach the 500 mm grid module to the first two beams. The beam spacing was 400 mm. Again, because the flange of the bottom chord of the truss was constant throughout the span, the adjustment plates were not installed (see Fig. 19). The 1000 mm grid module was then installed on the three beams. Two new L-beams were placed with 200 mm between the last beam and the next beam and 400 mm between the two new beams. A 500 mm wide grid module was placed, followed by a new L-beam 400 mm from the last one. Then the 500 mm wide grid module was replaced by a 1000 mm wide grid module, and two new stringers were installed with a distance of 200 mm between the last and the next beam and 400 mm between the two new stringers. Finally, the handrail was installed.

With this walkway, there are two options for inspection work: a) install it along the entire length of the bridge b) close off a 2.5 m walkway module laterally with a handrail, carry out inspection work in this area, and then move this module along the bridge, following the steps of the above methodology (see Fig. 24).

6.2. Fillaboa bridge

The second case study in which the proposed methodology was applied is the Fillaboa railway bridge over the Tea River in Salvaterra de Miño, Pontevedra, Spain (Fig. 20). It is a bridge currently in railway use, difficult to access, and in need of a structural health inspection due to its current state of corrosion. This bridge belongs to the railway called “Línea Férrea del Miño” and was built in 1877. The bridge has two identical spans, each 49.0 m long, 5.6 m wide, and 4.4 m high. Each span consists of two lateral trusses offset 5.0 m from each other. Nineteen modules of equal size form the lateral trusses, with the tenth module being the axis of symmetry of the truss.

6.2.1. Scanning of the construction

The Faro Focus 3D X 330 was used to scan the bridge. The first ten scans were performed (see positions in Fig. 21) with medium resolution (6.0 mm between measuring points at a distance of 10 m) with an average number of points per scan of 23,893,864, although the actual points belonging to the bridge were only 697,530 on average. Also, due to the dimensions of the bridge, with a total length of 100 m, four high-resolution scans were performed (3.0 mm between measuring points at a distance of 10 m) with an average number of points per scan of 106,933,165 points, although the actual points belonging to the bridge

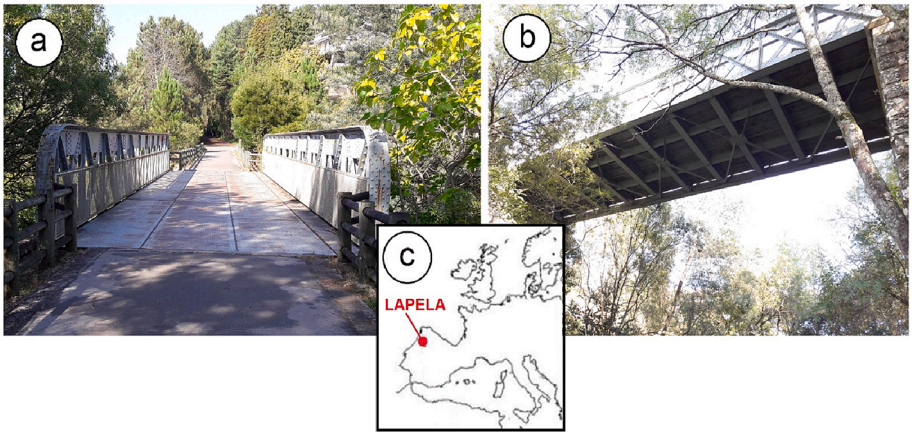

Fig. 15. Historic steel bridge over the Gadanha River a) View of the inside of the structure b) Map of the bridge site c) View of the underside of the structure.

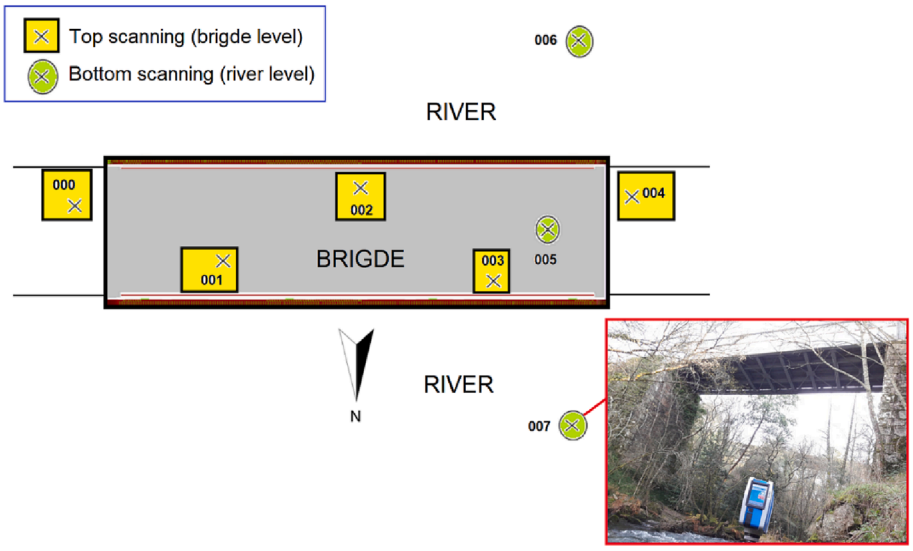

Fig. 16. Scheme of laser scan positions (plan view of the bridge).

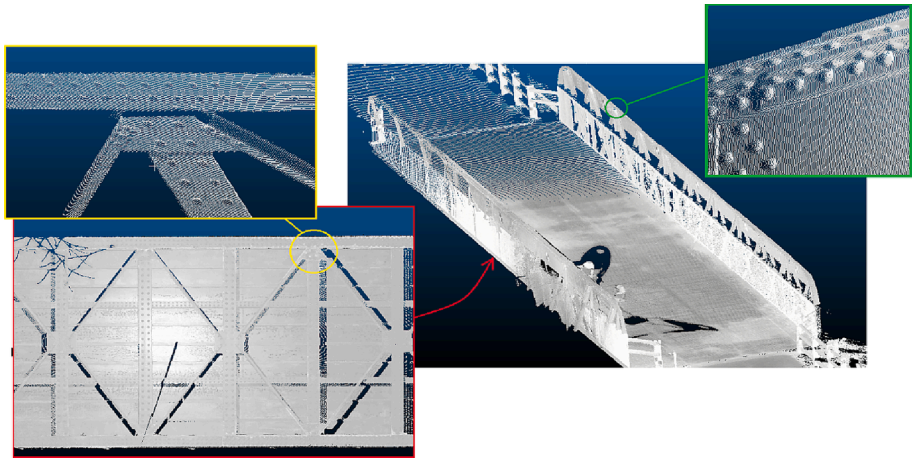

Fig. 17. LiDAR point cloud data of the steel bridge over the Gadanha River.

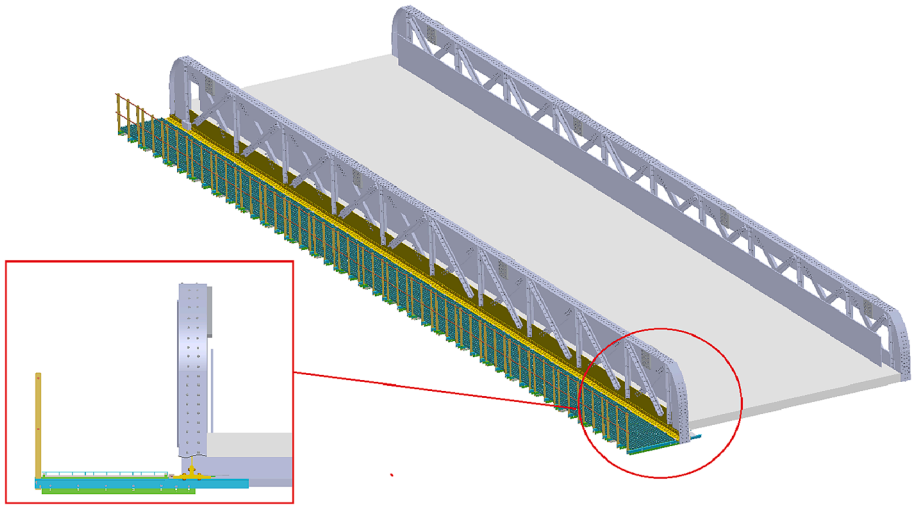

Fig. 18. 3D geometrical model of the steel bridge over the Gadanha River and subsequent assembly of the developed detachable walkway system.

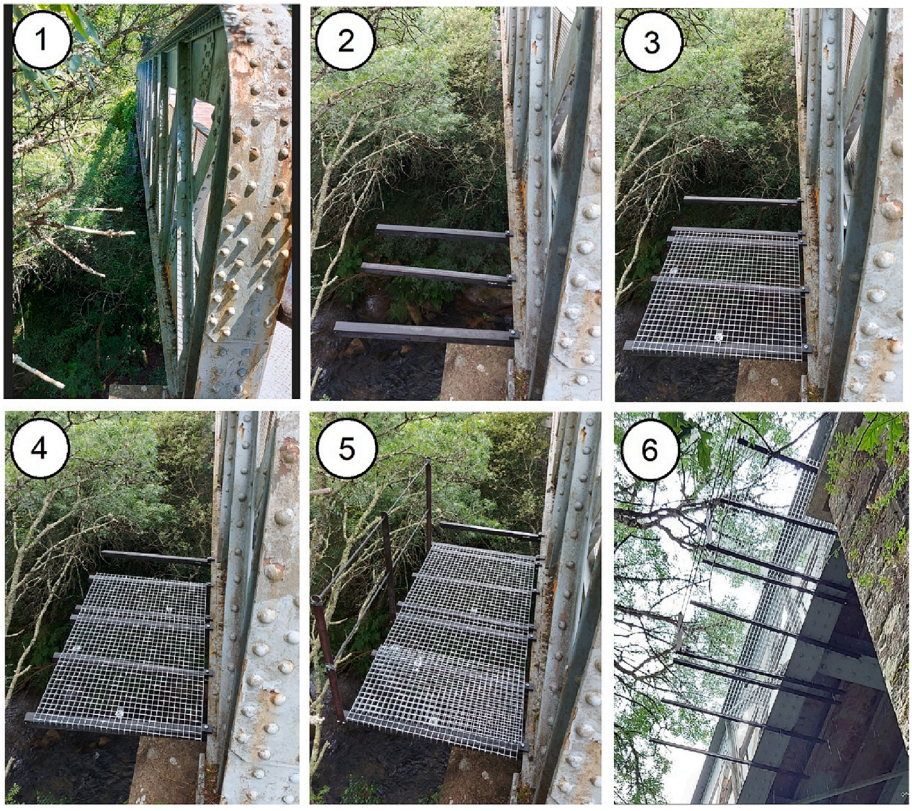

Fig. 19. Steps to assemble the developed detachable walkway system on the steel bridge over the Gadanha River.

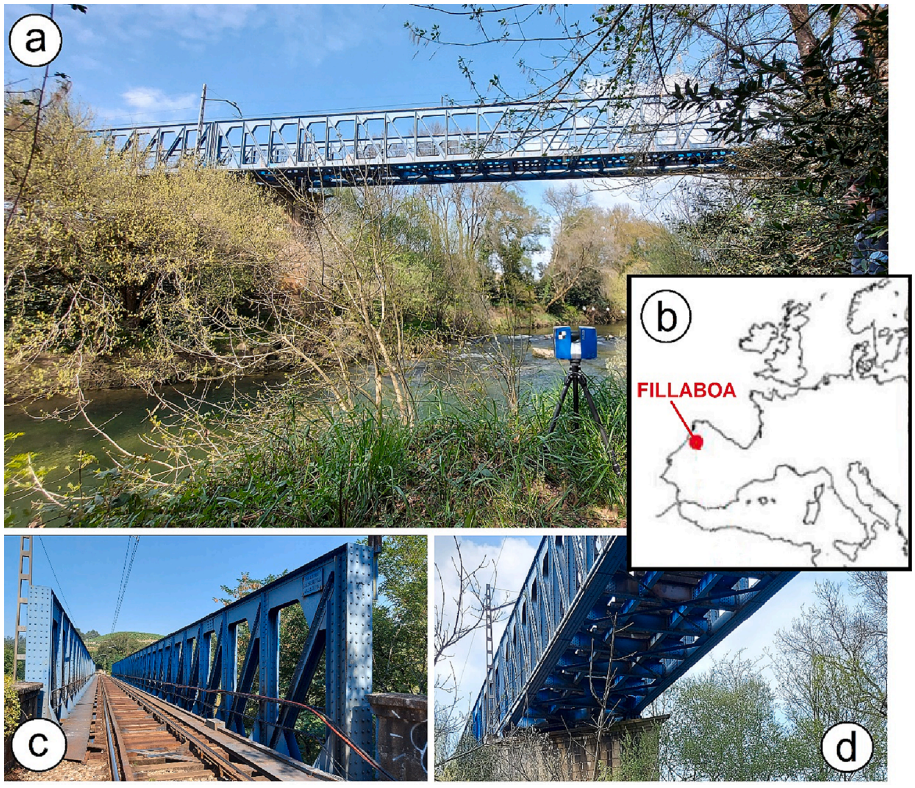

Fig. 20. Railway bridge over the Tea River a) Front view of the first span of the bridge b) Map of the bridge site c) View of the interior of the bridge d) Bottom view of the structure.

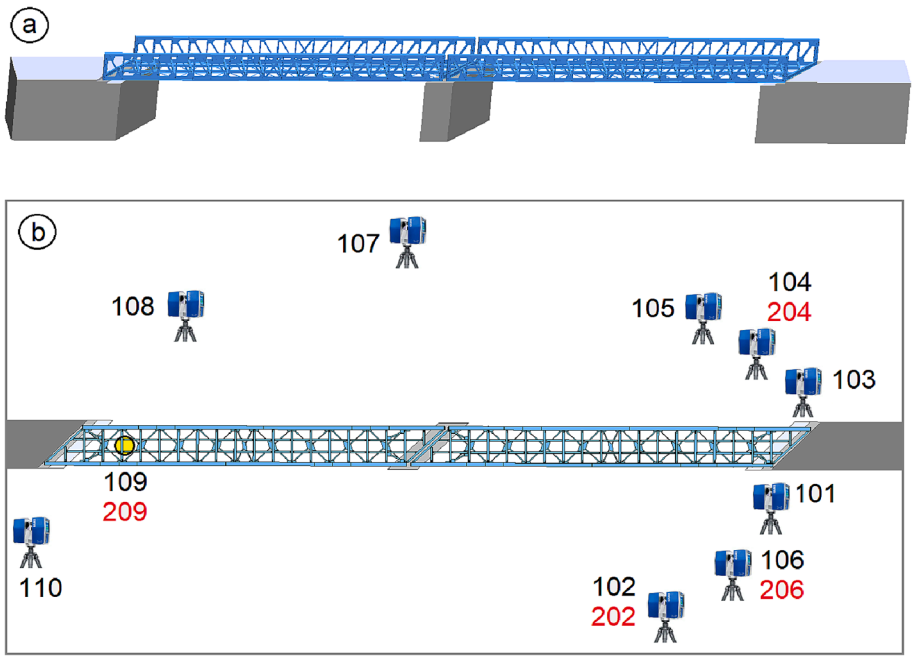

Fig. 21. a) 3D geometrical model of the Fillaboa Bridge b) Plan view of the laser scan positions and their nomenclature.

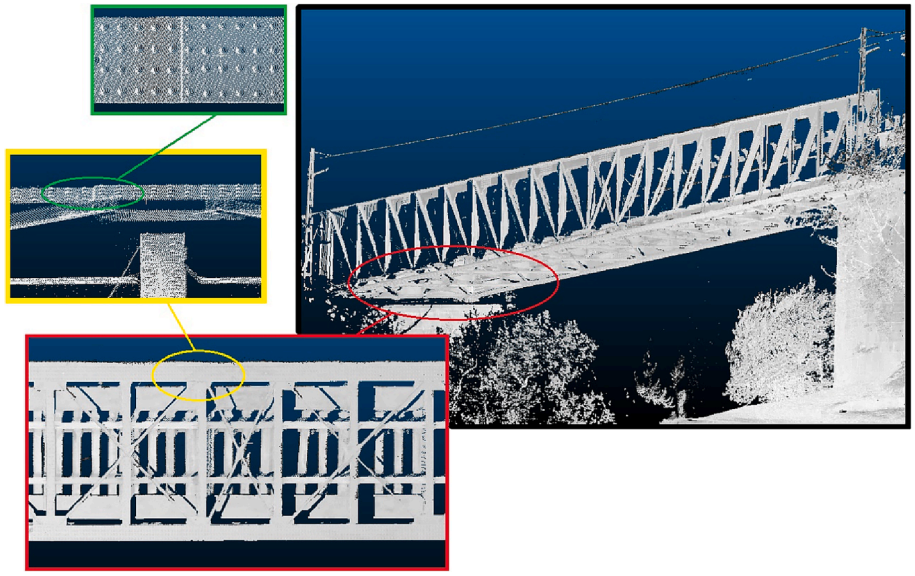

Fig. 22. LiDAR point cloud data of the Fillaboa bridge.

were only 3,924,607 on average.

6.2.2. LiDAR point cloud data

The measurements needed to study the assembly of the walkway were extracted from the LiDAR point clouds (Fig. 22). The scans used were Ref.101, 103, 110, 204, 206, and 209. Then, to obtain the complete 3D model of the bridge, the different point clouds were registered into a single point cloud with a single reference system. This way, the ten scans taken at half resolution were used, resulting in a final global point cloud of 29,610,362 points.

6.2.3. 3D modeling of the construction

Departing from the point cloud, the general 3D geometric modeling of the bridge was performed using Solidworks software. In order to check the error between the 3D model and the actual bridge, the parts of the geometric model related to the anchorage of the walkway were exported in "*. step" format, compatible with the point cloud processing software CloudCompare. The bottom of the longitudinal chords of the truss was checked, including the changes in thickness due to the number of steel plates used and the position of the rivets (Fig. 23). The 3D model was then aligned with the point cloud, and the error was compared using the *Cloud to Mesh* tool included in the software. This tool provides a histogram showing the deviation between the point cloud and the 3D model in each inspected area of the structure. Before assembling the walkways on the actual structure, the virtual assembly was performed on the 3D model (Fig. 24) to verify no interferences or errors.

6.2.4. Installation of the walkway

In this case study, a platform module was assembled to verify the functionality and ease of assembly and disassembly of the proposed

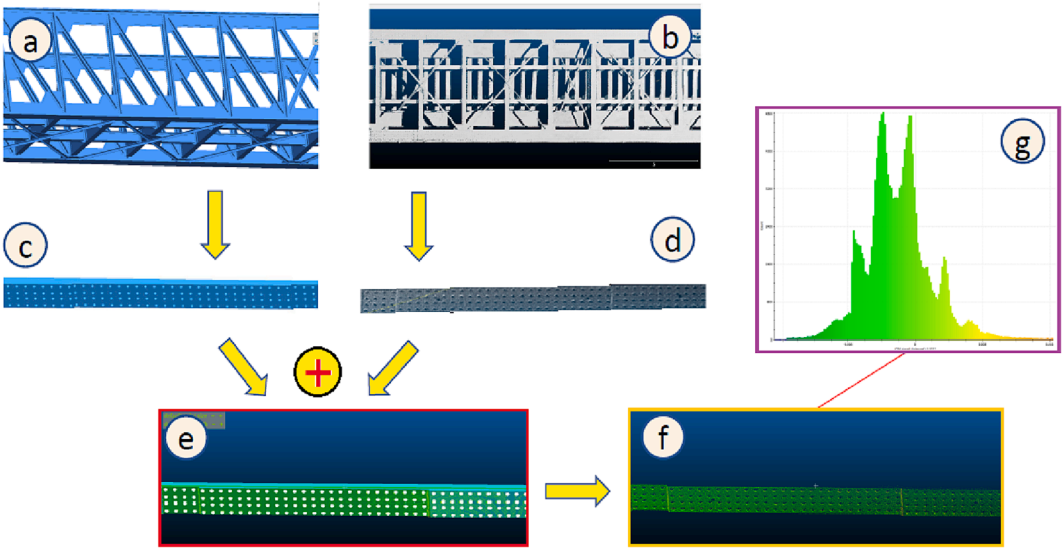

Fig. 23. Scheme of the process of comparing the critical parts of the 3D model of the walkway anchorage system with the point cloud a) 3D geometric model of the bridge b) General point cloud of the bridge c) 3D model of the lower chord of the truss d) Point cloud of the lower chord of the truss e) Alignment of the 3D model with the point cloud f) Point cloud with color scale according to the distance from the 3D model g) Histogram of the deviation between the point cloud and the model in the inspected area.

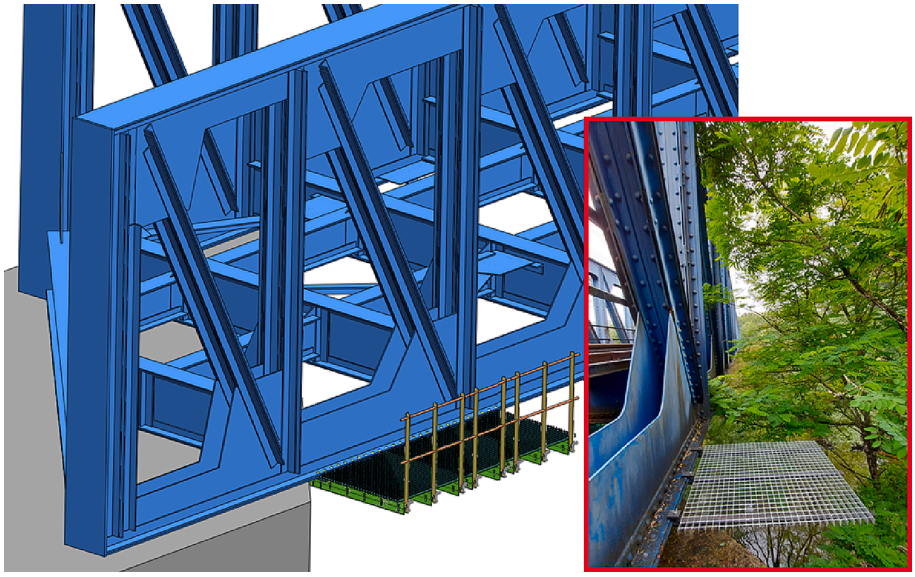

Fig. 24. a) 3D geometrical model of the Fillaboa bridge b) Assembly of a walkway module on the Fillaboa bridge.

walkway system (see Fig. 24). A single person assembled this module, and the steps followed are essentially the same as those used in the case of the bridge over the Gadanha river.

7. Conclusions

This work has developed a methodology and a system that, by combining non-invasive removable anchors with LiDAR techniques, allows the installation of easily assembled and disassembled walkways for structural health inspection, maintenance, repair, or accessibility in historic steel buildings without the need for additional scaffolding. The main innovations and advantages of the proposed and developed system are:

- The developed system allows the assembly and disassembly of the walkway from itself since a single person can easily manipulate all the components without the need for auxiliary equipment.
- With this walkway system, which uses clamps for anchoring, there is no need to perform invasive operations on the existing construction, such as welding or drilling to insert bolts.
- The system developed can be adapted to changes in the thickness of the flanges of the steel structural profiles where anchoring is required, and, thanks to the adjustment plate, it is possible to adjust each of the supports so that the walkway is perfectly level. This solution has proven to be adequate, although other designs, such as using FRP plates placed on the top of the L profile, could be studied as alternative solutions.
- Besides, due to the countersunk hole plate combined with the horizontal bolts of the clamps, it is possible to overcome the internal

areas of the structure where there are gusset plates that make it difficult to place a clamp.
- As observed from the FEM simulation results and experimental laboratory tests, the adjustment plate reinforces the L-girder, allowing it to support the loads required for a walkway of this type without using components too heavy for handling during assembly and disassembly.
- The developed platform system allows inspection, maintenance, and repair of the outside of the vertical trusses but does not allow inspection of the underside of the deck, which is also usually difficult to access. Future works should focus on developing similar easily assembled, disassembled, and reconfigurable systems, such as the one presented in this study, for inspection and maintenance of the underside of the deck.

Declaration of Competing Interest

The authors declare that they have no known competing financial interests or personal relationships that could have appeared to influence the work reported in this paper.

Acknowledgments

This paper is based on the ongoing research of the lead author's Ph. D. thesis, under preparation at the International Doctorate School of UNED (EIDUNED); the authors, therefore, wish to express their gratitude for that institution's support. This work has been supported by the Spanish Ministry of Science and Innovation through the project grant TED2021-130497A-I00, and co-financed by the H2020-NMBP-TO-IND program through the UE-H2020 with application code: H2020-NMBP-TO-IND 2020-958171 (IM-SAFE)

References

[1] Gocál J, Odrobiňák J. On the influence of corrosion on the load-carrying capacity of old riveted bridges. Materials 2020;13(3):717. https://doi.org/10.3390/ma13030717.
[2] Zhao Z, Gao T, Liu J, Dai B, Gao H. Local bearing capacity of steel beam webs with random pit corrosion. Structures 2023;48:1259–70.
[3] Di Sarno L, Majidian A, Karagiannakis G. The Effect of Atmospheric Corrosion on Steel Structures: A State-of-the-Art and Case-Study. Buildings 2021;11(12):571. https://doi.org/10.3390/buildings11120571.
[4] Li H, Shen L, Deng S. A Generalized Framework for the Alternate Load Path Redundancy Analysis of Steel Truss Bridges Subjected to Sudden Member Loss Scenarios. Buildings 2022;12(10):1597. https://doi.org/10.3390/buildings12101597.
[5] Lazorenko G, Kasprzhitskii A, Nazdracheva T. Anti-corrosion coatings for protection of steel railway structures exposed to atmospheric environments: A review. Constr Build Mater 2021;288:123115. https://doi.org/10.1016/j.conbuildmat.2021.123115.
[6] Ghiasi A, Ng C-T, Sheikh AH. Damage detection of in-service steel railway bridges using a fine k-nearest neighbor machine learning classifier. Structures 2022;45:1920–35.
[7] Guo S, Si R, Dai Q, You Z, Ma Y, Wang J. A critical review of corrosion development and rust removal techniques on the structural/environmental performance of corroded steel bridges. J Clean Prod 2019;233:126–46. https://doi.org/10.1016/j.jclepro.2019.06.023.
[8] Chmielewski, R., & Muzolf, P. (2021). Analysis of degradation process of a railway steel bridge in the final period of its operation. Structure and Infrastructure Engineering, 1-17. https://doi.org/ 10.1080/15732479.2021.1956550.
[9] Groover MP. (2010) Fundamentals of Modern Manufacturing. fourth ed. USA: John Wiley & Sons Inc; 2010.
[10] Kalpakjian S, Schmid SR. (2006) Manufacturing, Engineering and Technology, 6th Edition-Serope. USA: Prentice-Hall; 2006.
[11] Pongiglione M, Calderini C, D'Aniello M, Landolfo R. Novel reversible seismic-resistant joint for sustainable and deconstructable steel structures. J Build Eng 2021;35:101989. https://doi.org/10.1016/j.jobe.2020.101989.
[12] Cabaleiro M, Comesaña R, González-Gaya C, Caamaño C. Analytical Model for the Fatigue Analysis of Steel Joints by Clamps According to the Lever Length. Materials 2021;14(24):7726. https://doi.org/10.3390/ma14247726.
[13] Cabaleiro M, Conde B, Riveiro B, Caamaño JC. Analysis of steel connections with girder clamps according to the bolts preload. J Constr Steel Res 2020;168:105866. https://doi.org/10.1016/j.jcsr.2019.105866.
[14] Cabaleiro M, Riveiro B, Conde B, Caamaño JC. Analytical T-stub model for the analysis of clamps in structural metal joints. J Constr Steel Res 2017;130:138–47. https://doi.org/10.1016/j.jcsr.2019.105866.
[15] Boddupalli C, Sadhu A, Rezazadeh Azar E, Pattyson S. Improved visualization of infrastructure monitoring data using building information modeling. Struct Infrastruct Eng 2019;15(9):1247–63. https://doi.org/10.1080/15732479.2019.1602150.
[16] Kassotakis N, Sarhosis V. Employing non-contact sensing techniques for improving efficiency and automation in numerical modelling of existing masonry structures: A critical literature review. Structures 2021;32:1777–97.
[17] Pellis, E., Masiero, A., Tucci, G., Betti, M., & Grussenmeyer, P. (2021). Assembling an image and point cloud dataset for heritage building semantic segmentation. International Archives of the Photogrammetry, Remote Sensing and Spatial Information Sciences, 46, 539-546. https://doi.org/ 10.5194/isprs-archives-XLVI-M-1-2021-539-2021.
[18] Riveiro B, Lourenço PB, Oliveira DV, González-Jorge H, Arias P. Automatic morphologic analysis of quasi-periodic masonry walls from LiDAR. Comput Aided Civ Inf Eng 2016;31(4):305–19. https://doi.org/10.1111/mice.12145.
[19] Garzia F, Costantino D, Baiocchi V. Security and safety management and role of laser scanning in unique and peculiar cultural heritage sites such as the papal basilica and the sacred convent of Saint Francis in Assisi in Italy. Heritage Architect Stud 2018;269. https://doi.org/10.2495/HA-V2-N2-271-282.
[20] Jasieńko, J., Raszczuk, K., Kleszcz, K., & Frąckiewicz, P. (2021, June). Numerical analysis of historical masonry domes: A study of St. Peter's Basilica dome. In *Structures* (Vol. 31, pp. 80-86). Elsevier. https://doi.org/10.1016/j.istruc.2021.01.082.
[21] Herráez J, Navarro P, Denia JL, Martín MT, Rodríguez J. Modeling the thickness of vaults in the church of Santa Maria de Magdalena (Valencia, Spain) with laser scanning techniques. J Cult Herit 2014;15(6):679–86. https://doi.org/10.1016/j.culher.2013.11.015.
[22] Acikgoz S, Soga K, Woodhams J. Evaluation of the response of a vaulted masonry structure to differential settlements using point cloud data and limit analyses. Constr Build Mater 2017;150:916–31. https://doi.org/10.1016/j.conbuildmat.2017.05.075.
[23] Pallarés FJ, Betti M, Bartoli G, Pallarés L. Structural health monitoring (SHM) and Nondestructive testing (NDT) of slender masonry structures: A practical review. Constr Build Mater 2021;297:123768. https://doi.org/10.1016/j.conbuildmat.2021.123768.
[24] Cuartero J, Cabaleiro M, Sousa HS, Branco JM. Tridimensional parametric model for prediction of structural safety of existing timber roofs using laser scanner and drilling resistance tests. Eng Struct 2019;185:58–67. https://doi.org/10.1016/j.engstruct.2019.01.096.
[25] Ozbek M. Smart Maintenance and Health Monitoring of Buildings and Infrastructure Using High-Resolution Laser Scanners. Buildings 2022;12(4):454. https://doi.org/10.3390/buildings12040454.
[26] Gyetvai N, Truong-Hong L, Laefer DF. Laser scan-based structural assessment of wrought iron bridges: Guinness Bridge, Ireland. Proc Inst Civil Eng-Eng History Heritage 2018;171(2):76–89. https://doi.org/10.1680/jenhh.17.00018.
[27] Xu, D., Wang, Y., Liu, X., Chen, B., & Bu, Y. (2023, March). A novel method and modelling technique for determining the initial geometric imperfection of steel members using 3D scanning. In *Structures* (Vol. 49, pp. 855-874). Elsevier. https://doi.org/10.1016/j.istruc.2023.01.136.
[28] Cabaleiro M, Riveiro B, Arias P, Caamaño JC. Algorithm for the analysis of deformations and stresses due to torsion in a metal beam from LIDAR data. Struct Control Health Monit 2016;23(7):1032–46. https://doi.org/10.1002/stc.1824.
[29] En,. Eurocode 3: Design of steel structures - Part 1–8: Design of joints. European Committee for Standard; 1993-1-8: 2005.
[30] EN 1991-1-1:2002. Eurocode 1: Actions on structures - Part 1-1: General actions - Densities, self-weight, imposed loads for buildings. European Committee for Standardization, Brussels, 2002.
[31] EN 1990:2002. Eurocode 0 - Basis of structural design. European Committee for Standardization, Brussels, 2002.
[32] Micro-measurement. D4 model. http://docs.micro-measurements.com/?id=2565 (accessed on 24/03/2023).
[33] Software Ansys 2022. Ansys | Engineering Simulation Software. https://www.ansys.com (accessed on 06/15/2022).
[34] EN 1090-2:2018. Execution of steel structures and aluminium structures - Part 2: Technical requirements for steel structures. European Committee for Standardization, Brussels, 2018.
[35] Faro Focus Laser Scaner. https://knowledge.faro.com/Hardware/Focus/Focus/Technical_Specification_Sheet_for_the_Focus_Laser_Scanner#Focus3D_X_30.2F130.2F330.2FHDR.